Component analysis of errors in satellite-based precipitation estimates

Yudong Tian,[1,2] Christa D. Peters-Lidard,[1] John B. Eylander,[3] Robert J. Joyce,[4] George J. Huffman,[5,6] Robert F. Adler,[5,7] Kuo-lin Hsu,[8] F. Joseph Turk,[9] Matthew Garcia,[1,10] and Jing Zeng[1,11]

Received 20 February 2009; revised 10 June 2009; accepted 25 August 2009; published 16 December 2009.

[1] Satellite-based precipitation estimates have great potential for a wide range of critical applications, but their error characteristics need to be examined and understood. In this study, six (6) high-resolution, satellite-based precipitation data sets are evaluated over the contiguous United States against a gauge-based product. An error decomposition scheme is devised to separate the errors into three independent components, hit bias, missed precipitation, and false precipitation, to better track the error sources associated with the satellite retrieval processes. Our analysis reveals the following. (1) The three components for each product are all substantial, with large spatial and temporal variations. (2) The amplitude of individual components sometimes is larger than that of the total errors. In such cases, the smaller total errors are resulting from the three components canceling one another. (3) All the products detected strong precipitation (>40 mm/d) well, but with various biases. They tend to overestimate in summer and underestimate in winter, by as much as 50% in either season, and they all miss a significant amount of light precipitation (<10 mm/d), up to 40%. (4) Hit bias and missed precipitation are the two leading error sources. In summer, positive hit bias, up to 50%, dominates the total errors for most products. (5) In winter, missed precipitation over mountainous regions and the northeast, presumably snowfall, poses a common challenge to all the data sets. On the basis of the findings, we recommend that future efforts focus on reducing hit bias, adding snowfall retrievals, and improving methods for combining gauge and satellite data. Strategies for future studies to establish better links between the errors in the end products and the upstream data sources are also proposed.

Citation: Tian, Y., C. D. Peters-Lidard, J. B. Eylander, R. J. Joyce, G. J. Huffman, R. F. Adler, K. Hsu, F. J. Turk, M. Garcia, and J. Zeng (2009), Component analysis of errors in satellite-based precipitation estimates, *J. Geophys. Res.*, *114*, D24101, doi:10.1029/2009JD011949.

1. Introduction

[2] Accurate measurement of global precipitation is critical to many applications, such as climate studies, agricultural forecasts, natural hazards and hydrology. Especially for land surface hydrology, errors in precipitation measurements can cause significant uncertainties in predicting processes such as surface runoff [e.g., *Nijssen and Lettenmaier*, 2004; *Tian et al.*, 2006] and land slides [*Hong et al.*, 2007], because of the highly nonlinear nature of these physical processes [e.g., *Ogden and Julien*, 1993; *Nykanen et al.*, 2001].

[3] Currently satellite-based remote sensing is essential in producing estimates of global precipitation. By combining as many satellite platforms as available, one can obtain a global coverage of precipitation observation with high spatial and temporal resolutions (0.5 degree, daily or higher). Most of the recent high-resolution global products are produced roughly this way, albeit each of them has its unique approaches in cross-calibrating, weighting, and blending the various data sources. Some of these multi-

[1]Hydrological Sciences Branch, NASA Goddard Space Flight Center, Greenbelt, Maryland, USA.
[2]Also at Goddard Earth Sciences and Technology Center, University of Maryland Baltimore County, Baltimore, Maryland, USA.
[3]Air and Space Models Integration Branch, Air Force Weather Agency, Offutt Air Force Base, Nebraska, USA.
[4]Climate Prediction Center, NCEP, NWS, NOAA, Camp Springs, Maryland, USA.
[5]Laboratory for Atmospheres, NASA Goddard Space Flight Center, Greenbelt, Maryland, USA.
[6]Also at Science Systems and Applications, Inc., Lanham, Maryland, USA.
[7]Also at Earth System Science Interdisciplinary Center, University of Maryland, College Park, Maryland, USA.
[8]Center for Hydrometeorology and Remote Sensing, Department of Civil and Environmental Engineering, University of California, Irvine, California, USA.
[9]Marine Meteorology Division, Naval Research Laboratory, Monterey, California, USA.
[10]Now at Department of Hydrology and Water Resources, University of Arizona, Tucson, Arizona, USA.
[11]Also at Science Applications International Corporation, Beltsville, Maryland, USA.

Copyright 2009 by the American Geophysical Union.
0148-0227/09/2009JD011949

sensor products also incorporate ground-based measurements, such as gauge data.

[4] For useful application of these data sets, their quality has to be evaluated and error characteristics analyzed. Such evaluation and analysis will give better guidance to users in selecting a product for their particular applications, and help them assess the impact of the errors on these applications. Equally importantly, if such error analysis could yield insight into the sources of the errors and how to correct or reduce them, it would be greatly helpful to the algorithm developers and data producers for further improvement.

[5] There have been many evaluation efforts, exemplified by the Algorithm Intercomparison Programme (AIP) [*Arkin and Xie*, 1994; *Ebert et al.*, 1996], the Precipitation Intercomparison Project (PIP) [*Smith et al.*, 1998; *Adler et al.*, 2001] and the more recent Program to Evaluate High Resolution Precipitation Products (PEHRPP) [*Arkin and Turk*, 2006]. More recent examples include *Gottschalck et al.* [2005], who compared several satellite-based, surface gauge-based and model data over contiguous U. S. (CONUS), documented the errors and studied the impact on land surface modeling; *Ebert et al.* [2007], who examined several high-resolution precipitation data sets from satellite-based estimates and from numerical weather prediction models, over CONUS, Australia and Europe, and found satellite-based estimates performed well in summer; *Tian et al.* [2007], who studied two leading Tropical Rainfall Measuring Mission (TRMM)–based satellite products over a wide range of time scales, from seasonal climatology to diurnal, and documented the error characteristics over CONUS and the southeastern United States in particular; and more recently, *Hossain and Huffman* [2008], who evaluated four satellite products over two smaller regions within CONUS. Studies over other areas with multiple satellite-based products have also been performed. *Ebert et al.* [2007] found that CMORPH (see section 3) has best probability of detection or temporal correlation over Australia and over the United Kingdom among other products. *Ruane and Roads* [2007] studied the variance of 3B42, CMORPH and PERSIANN (see section 3) over the globe, and found interesting differences among them. However, it is not clear which one performs better because of the lack of reliable global validation data. *Sapiano and Arkin* [2009] evaluated four of the six products to be studied here over the midwest United States and the tropical Pacific Ocean. Their analysis shows that these products tend to overestimate precipitation over the land region, especially in summer, and underestimate over the tropical ocean.

[6] Conceptually, satellite-based precipitation retrieval normally involves two steps, be it infrared (IR)-based [*Vicente et al.*, 1998], passive microwave (PMW)–based [*Ferraro et al.*, 1998], or a combination of the two [e.g., *Kidd et al.*, 2003]. The first step is the discrimination, or screening process, i.e., detection of raining and nonraining areas. Once the screening is done, the magnitude of the rain is estimated on the basis of empirical or physical relations between the signals (such as brightness temperature) and precipitation rate in the second step. Errors can take place in either step. During the screening step, if some raining areas are not detected, it will result in missed precipitation in the estimates. Conversely, some nonraining areas may be mistaken as raining ones, for example, by cold cloud top temperatures of high-level cirrus, or by false signatures produced from certain land surface features [*Grody*, 1991; *Tian and Peters-Lidard*, 2007], causing false precipitation. Finally, even when a raining area is correctly detected, there are still errors in accurately estimating the rain rate in the second step. Therefore, it would be very helpful to separate the errors into components associated with these retrieval stages, and help data producers and algorithm developers better trace the errors and reduce them.

[7] In this article, we devised a scheme to separate the total errors in a satellite-based data set into three independent components, hit bias, missed precipitation and false precipitation, which have close correspondence to the satellite retrieval processes described above. We applied this error decomposition scheme to six high-resolution satellite-based precipitation data sets, namely AFWA, TMPA (3B42), TMPA-RT (3B42RT), CMORPH, PERSIANN and NRL (see section 3), currently the most extensive collection of IR-PMW merged products. Our analysis produced the spatiotemporal distribution of these error components and their magnitudes for each product. Such an error decomposition yields less ambiguous assessment for data producers to infer the origin of the errors and for users to understand the unique and common strengths and weaknesses among the six products. It is also interesting to see the amplitudes of the three individual components are often larger than the total error; therefore it is not enough to evaluate a data set's performance solely on the basis of its total error, as most existing studies do. We hope these results not only give a broader perspective of the current state of precipitation remote sensing, but also provide more insight to both data users and producers for their application and further improvement of these products.

[8] The error decomposition scheme is introduced in section 2. The six satellite-based data sets, as well as a surface rain gauge-based product used as validation data, are described in section 3. Section 4 presents the results, including spatial and temporal characteristics and intensity distribution of the total error and its components, for each product. Finally, the results are summarized in section 5, with recommendations for possible future improvements in satellite-based precipitation estimates, based on the findings in this study.

2. Error Decomposition

[9] Given a precipitation field, $R(\vec{x},t)$, one can derive a binary-valued precipitation event mask, $P(\vec{x},t)$,

$$P(\vec{x},t) = \begin{cases} 1 & \text{if } R(\vec{x},t) > 0 \\ 0 & \text{if } R(\vec{x},t) = 0 \text{ or missing} \end{cases} \tag{1}$$

In practice, a small value (e.g., 1 mm/d) instead of 0 is usually used as the rain/no-rain threshold to determine the mask.

[10] Then when we evaluate a satellite-estimated precipitation field $R_2(\vec{x},t)$ against a reference data set, or "observations," $R_1(\vec{x},t)$, with their respective event masks, $P_2(\vec{x},t)$ and $P_1(\vec{x},t)$, we can define a hit mask:

$$P_{12} = P_1 \times P_2;$$

Table 1. Summary of Six Satellite-Based and One Gauge-Based Data Sets Used

Data Set	Full Name	Spatial Resolution	Temporal Resolution	Sensor Platforms	References
AFWA	Air Force Weather Agency's Agricultural Meteorology modeling system	0.5°	3 h	IR, SSM/I, WMO gauges, climatology	Data Format Handbook for AGRMET
3B42	TRMM Multisatellite Precipitation Analysis research product 3B42 Version 6	0.25°	3 h	IR, SSM/I, TRMM, AMSU-B, AMSR-E, gauges	*Huffman et al.* [2007]
3B42RT	TRMM Multisatellite Precipitation Analysis Real-time experimental product 3B42RT	0.25°	3 h	IR, SSM/I, TRMM, AMSU-B, AMSR-E	*Huffman et al.* [2009]
CMORPH	NOAA Climate Prediction Center (CPC) MORPHing technique	0.25°	3 h	IR, SSM/I, TRMM, AMSU-B, AMSR-E	*Joyce et al.* [2004]
PERSIANN	Precipitation Estimation from Remotely Sensed Information using Artificial Neural Networks	0.25°	3 h	IR, TRMM	*Hsu et al.* [1997] and *Sorooshian et al.* [2000]
NRL	Naval Research Laboratory's blended technique	0.25°	3 h	IR, VIS, SSM/I, TRMM, AMSU-B, AMSR-E	*Turk and Miller* [2005]
Higgins	NOAA CPC near-real-time daily precipitation analysis	0.25°	24 h	gauges	*Higgins et al.* [2000]

a miss mask:

$$P_{1\bar{2}} = P_1 \times P_{\bar{2}};$$

and a false alarm mask:

$$P_{\bar{1}2} = P_{\bar{1}} \times P_2;$$

where $P_{\bar{n}}$ denotes the Boolean complement of a binary mask P_n. The three masks are essentially what are used in calculating the conventional contingency table and accuracy measures, such as probability of detection, false alarm ratio and threat scores [e.g., *Wilks*, 1995]. A hit is an event when both the evaluated data and the reference data report precipitation coincidently. A miss (false alarm) is an event when the evaluated data report no precipitation (precipitation) while the reference data report otherwise.

[11] It is easy to see that the three masks above are "orthogonal," or independent, to one another:

$$P_{12} \times P_{1\bar{2}} = P_{12} \times P_{\bar{1}2} = P_{1\bar{2}} \times P_{\bar{1}2} = 0. \tag{2}$$

If we define total error, E, hit error, H, missed precipitation, $-M$, and false precipitation, F, as,

$$E = R_2 - R_1, \tag{3}$$

$$\begin{aligned} H &= (R_2 - R_1) \times P_{12} = H_2 - H_1, \\ -M &= -R_1 \times P_{1\bar{2}}, \\ F &= R_2 \times P_{\bar{1}2}. \end{aligned} \tag{4}$$

We use H_2 and H_1 in equation (4) to denote "hit precipitation in satellite estimates" and "hit precipitation in observations" to indicate the subsets consisting of coincidental precipitation within the satellite estimates and within the observations, respectively. Because of (2), H, $-M$ and F are independent to one another, and it can be shown that,

$$\begin{aligned} H - M + F &= (R_2 - R_1) \times P_{12} - R_1 \times P_{1\bar{2}} + R_2 \times P_{\bar{1}2} \\ &= R_2\left(P_{12} + P_{\bar{1}2}\right) - R_1\left(P_{12} + P_{1\bar{2}}\right) \\ &= R_2 \times P_2 - R_1 \times P_1 \\ &= R_2 - R_1 \\ &= E \end{aligned} \tag{5}$$

which means the total error E can be completely decomposed into three independent parts: hit error H, missed precipitation $-M$ and false precipitation F. Equation (5) still holds when spatial and temporal averaging are applied, but the total error and hit error will be called total bias and hit bias by convention.

[12] The relation $E = H - M + F$ raises a critical point. It implies that it is not enough to look at the total bias E as an indicator of the performance. The three individual components H, $-M$, and F could have larger amplitudes than the total error E, but they could cancel one another, resulting in total bias smaller than some of the components. This is especially true for $-M$ and F, which always have opposite signs. Therefore it is important to realize that the amplitude of the total bias alone is not enough to serve as a measure of the performance of a set of estimates; one needs to look at the three components as well to truly understand the error characteristics. Section 4 provides ample examples to illustrate this situation.

[13] *Berg et al.* [2006] employed a similar decomposition to compare collocated TRMM TMI and precipitation radar (PR) retrievals at pixel levels over ocean. *Ebert and McBride* [2000] used a scheme to decompose the errors into location error, rain volume error and pattern error for verification of numerical model forecasts. It would be

interesting to compare the two different schemes applied to satellite-based estimates in future studies.

3. Data

[14] Six satellite-based precipitation data sets and one surface rain gauge-based product are used in our study. We denote the six satellite-based data sets as AFWA, (TMPA) 3B42, (TMPA) 3B42RT, CMORPH, PERSIANN and NRL, and the surface rain gauge product as Higgins. Except AFWA, all the satellite-based data sets have a 0.25 by 0.25 degree spatial resolution and a 3-h temporal resolution. See Table 1 for a summary including these products' full names, basic features and references for further information.

[15] AFWA refers to the data set from the Air Force Weather Agency (AFWA)'s Agriculture Meteorology modeling system (AGRMET), one of the leading operational land surface modeling systems which has been in operation for 2 decades. It assimilates a wide array of input data sources, including real time precipitation observations and analyses, global model forecasts, and satellite remote sensing data, to provide timely estimates of global precipitation, soil moisture and soil temperature etc. More information can be found in the Data Format Handbook for AGRMET, available at http://www.mmm.ucar.edu/mm5/documents/DATA_FORMAT_HANDBOOK.pdf.

[16] AFWA precipitation is a multisensor product, merging surface reports, remote sensing data, cloud analysis and climatology. As far as the tropics and midlatitudes are concerned, AFWA is essentially a satellite-based, gauge-corrected product composed of retrievals from IR channels on geostationary platforms and PMW channels on polar orbiting ones, overlaid by gauge analysis. Surface gauge reports from the World Meteorological Organization (WMO)'s Global Telecommunication System (GTS) network are used wherever available, with the Barnes [*Barnes*, 1964] analysis scheme. Over CONUS AFWA usually receives about 1000 gauge reports daily. When there are multiple data sources at a grid box, a predefined precedence (gauge analysis, then PMW and lastly IR) is used to determine which data source is used exclusively.

[17] TMPA 3B42 (Version 6) and 3B42RT are two of the Tropical Rainfall Measuring Mission (TRMM) Multisatellite Precipitation Analysis (TMPA) products provided by NASA Goddard Space Flight Center [*Huffman et al.*, 1997, 2007, 2009]. Both 3B42 and 3B42RT derive their precipitation estimates primarily by merging the most recent PMW scans available from the array of sensors including the TRMM Microwave Imager (TMI), the Special Sensor Microwave Imager (SSM/I), the Advanced Microwave Sounding Unit-B (AMSU-B) and the most recent Advanced Microwave Scanning Radiometer–Earth Observing System (AMSR-E). Both data sets use IR-based retrievals from geostationary satellites as well, to fill PMW coverage gaps. In addition, 3B42 incorporates global surface gauge measurements on a monthly basis for bias correction, while 3B42RT does not contain any gauge information, and is regarded as an experimental product with an evolving algorithm. In particular, 3B42RT data prior to 3 February 2005 are considered obsolete because they result from an early version of the algorithm that was diagnosed as having major problems in wintertime over land surface. Therefore results presented here for 3B42RT before February 2005 only serve as historical context. Both products have been used in many applications such as land data assimilation [e.g., *Gottschalck et al.*, 2005] and landslide prediction [*Hong et al.*, 2007].

[18] CMORPH refers to the National Centers for Environmental Prediction (NCEP)'s Climate Prediction Center (CPC) MORPHing technique [*Joyce et al.*, 2004; *Janowiak et al.*, 2005]. This technique uses the high-resolution IR imagery to infer the motion of rainfall patterns between PMW scans, and use this advection information to obtain a smooth "morphing" of PMW rain patterns between PMW snapshots. The PMW-based retrievals are from almost the same set of sensors as 3B42 and 3B42RT. CMORPH used in this study has a spatial resolution of 0.25 by 0.25 degree and a time resolution of 3 h (although a higher-resolution 8 km, hourly CMORPH is also available).

[19] PERSIANN (Precipitation Estimation from Remotely Sensed Information using Artificial Neural Networks) [*Hsu et al.*, 1997, 1999; *Sorooshian et al.*, 2000] is a neural network-based system for estimating precipitation from remotely sensed data. It uses IR imagery from geostationary satellites to derive precipitation, while its parameters are regularly adjusted using PMW-based estimates from TMI and SSM/I.

[20] NRL refers to the Naval Research Laboratory (NRL)'s blended technique [*Turk and Miller*, 2005]. It uses coincident and collocated infrared and PMW pixels aggregated to 2 by 2 degree grid boxes to calculate IR rainfall threshold and rain rate distribution. The IR rainfall data are then regridded onto a global 0.1 degree grid and weighted mean is used to combine the PMW and calibrated IR data.

[21] The Higgins data set ("observations") used as ground-based reference is the NCEP CPC near–real time daily precipitation analysis [*Higgins et al.*, 2000]. This data set is derived from the daily reports of 6000–7000 CPC Cooperative rain gauges over CONUS, with quality control measures including duplicate station checks, neighbor checks and standard deviation checks against climatology. The station data are projected on a 0.25 by 0.25 degree grid with a modified *Cressman* [1959] analysis scheme. It also uses ground-based radar estimates to eliminate unrepresentative zeros reported by a small portion of the gauges. We also derived a 0.5 degree version to facilitate comparison with AFWA.

[22] It is worth noting that the Higgins gauge data are certainly not perfect "truth." The undercatch problem for rain gauges, especially during winter and in mountainous regions, is well documented [e.g., *Legates and DeLiberty*, 1993]. In addition, projecting data from point-scale gauge measurements tends to spatially smooth and potentially depict precipitation areas as more expansive than is true. This is illustrated by the extensive light drizzle (<1mm/d) as shown in the gray shadings in Figure 1. In this study, we use 1 mm/d as the rain/no rain threshold to eliminate the effect of these drizzles, which account for less than 3% of total rainfall for the rainy days shown in Figure 1, and are also below the detection threshold of the satellite algorithms.

[23] To assess the amplitude of the uncertainties in the gauge data, we intercompared Higgins data with NCEP's Next-Generation Weather Radar (NEXRAD) Stage IV data

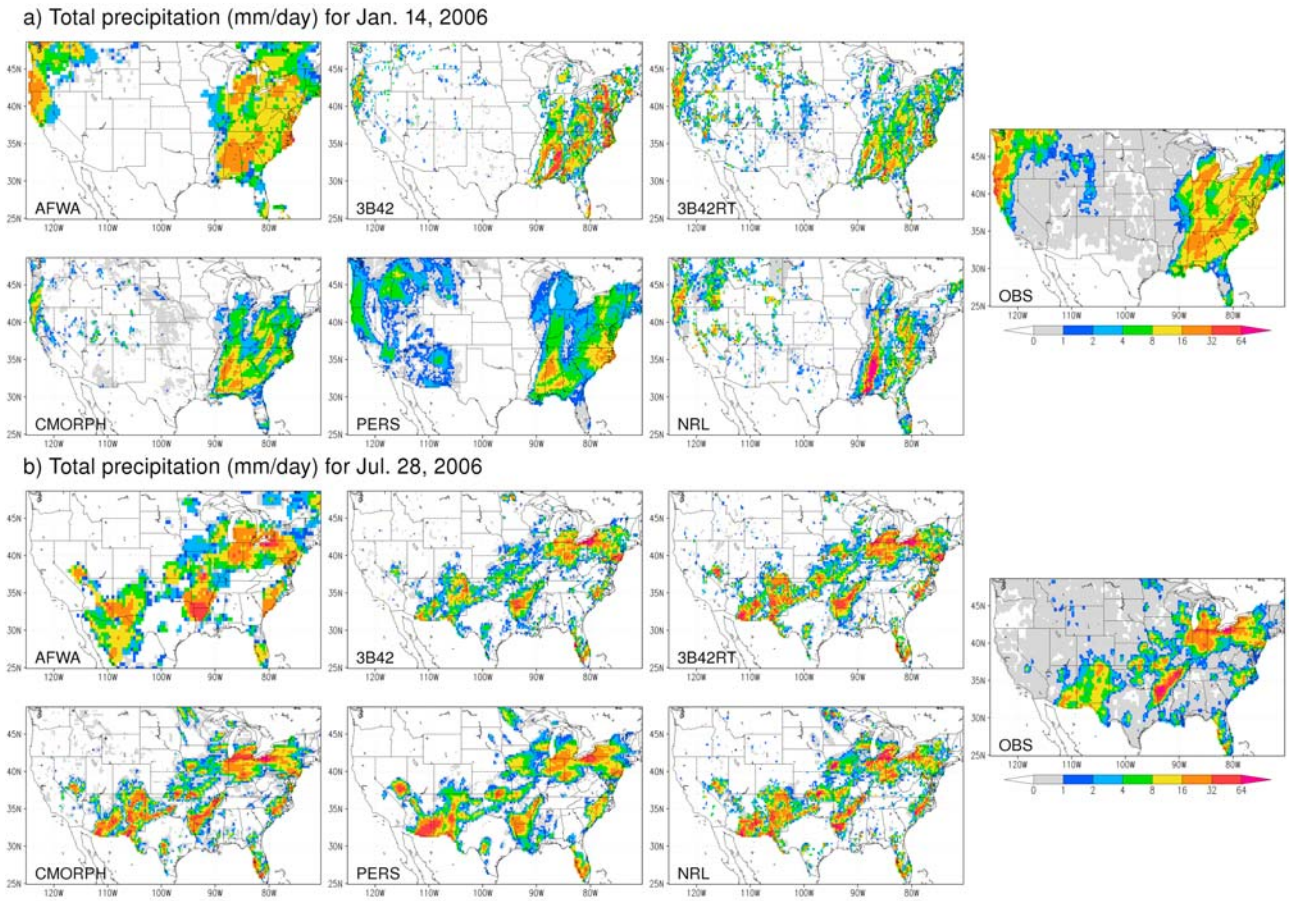

Figure 1. Sample daily precipitation patterns from each data set for (a) a winter day (14 January 2006) and (b) a summer day (28 July 2006).

[*Lin and Mitchell*, 2005], and a more recent gauge-based analysis, the CPC Unified gauge analysis [*Chen et al.*, 2008], which uses a different algorithm to project the station data onto the grid and collects slightly more station reports. Over the eastern CONUS, the differences between them are small, especially for strong precipitation events (>20 mm/d). Because of the high density of the gauges in this region, we estimate the errors in the gauge data is one order of magnitude lower than those in the satellite data. Therefore the errors in gauge data in the eastern CONUS will not qualitatively impact the evaluation of the current generation of satellite-based estimates, especially on the temporal and spatial scales used in this study. In the western CONUS, however, the uncertainties become much larger, especially in winter. Stage IV data severely underestimate relative to either gauge data set, mainly because of the complex terrain. Meanwhile, *Pan et al.* [2003] show Higgins data also underestimate by nearly 60%, an error amplitude similar to those of the satellite-based data sets (see Table 2). Consequently, over the western CONUS, missed precipitation and negative hit biases tend to be severely underestimated, and false precipitation and positive hit biases overestimated, by roughly a factor of 2.

[24] We selected a common time span from June 2003 through February 2007, as our study period. This period contains four summers (June, July, and August (JJA)) and four winters (December, January, and February (DJF)), except for NRL, which does not have data available for the first summer and first winter. All the satellite data sets are aggregated to daily accumulation for comparison with Higgins. Special attention was paid to match up the different spatial and temporal grids used in each data set. For example, Higgins's 0.25 degree grid has a half-grid shift from the 0.25 degree grid used by the satellite-based data

Table 2. Seasonally Averaged Error Components as Percentages of Total Observed (Higgins) Precipitation[a]

Product	H (%)	$-M$ (%)	F (%)	$E = H - M + F$ (%)
		Winter (DJF)		
AFWA	−2.5	−17.2	7.8	−11.9
3B42	0.7	−34.0	12.8	−20.6
3B42RT	9.9	−27.9	47.0	29.0
CMORPH	−21.7	−39.5	6.6	−54.5
PERSIANN	−1.3	−22.0	28.7	5.4
NRL	−10.9	−32.0	42.7	−0.1
		Summer (JJA)		
AFWA	16.8	−18.2	11.7	10.2
3B42	3.5	−19.1	6.0	−9.6
3B42RT	53.2	−20.5	15.1	47.9
CMORPH	49.9	−12.2	13.4	51.1
PERSIANN	34.8	−15.0	18.1	37.9
NRL	41.1	−24.4	14.3	31.0

[a]The seasonal average is over the 4 year (3 for NRL) period from JJA03 to DJF07.

sets. Therefore we chose to regrid Higgins data to the satellite 0.25 degree grid.

[25] Figure 1 shows sample daily precipitation patterns from each of the six satellite-based data sets and the Higgins data set (gauge data, or "OBS"), for a winter day (14 January 2006; Figure 1a) and a summer day (28 July 2006; Figure 1b). The winter day has two large-scale, strong precipitation systems present in the gauge data, one in the northwest coastal region, and the other, a V-shaped system, in the eastern United States. For this winter day, most satellite-based products captured the precipitation distribution in the east, but the V-shaped pattern was not well reproduced. The strong system over the northwest coastal region, and the light precipitation patch over the Rockies, are either mostly missed or only partially captured by the satellite-based products for this particular day. As to be shown in section 4, missed precipitation like this is typical in winter, and is the major source of negative biases in the western United States.

[26] For the summer day sample (Figure 1b), all the satellite-based data sets perform well in capturing the continent-scale, clustered precipitation pattern; no major features are missed by the satellite-based data. Still, there are differences in the amplitudes of the precipitation clusters among the data sets. Again, as will be shown in section 4, in summer, the amplitude differences in precipitation patterns become the leading error source for the satellite-based data.

4. Results

[27] The results of our error analysis are organized into three parts in this section: the spatial characteristics of the error components for each product for both summer and winter seasons; the spatially averaged error components on the daily scale over the whole 4 year period; and the distribution of the error components as a function of precipitation intensity. These three aspects will provide a relatively complete picture of the error characteristics for each product.

4.1. Spatial Analysis of Error Components

[28] For each product, we decomposed the total bias for each day over CONUS, and then accumulated the daily error components as well as the total errors into seasonal time scale for the 4 summers and winters (3 for NRL). In this article, we only present one winter (December 2005 and January and February 2006 (DJF06)) and one summer (June, July, and August 2006 (JJA06)) for each of the six data sets as representative examples, though interannual variations for each particular product are present. The results shown in section 4.2 will illustrate such variations.

[29] Figures 2 and 3 present the spatial patterns of the error components for DJF06 and JJA06, respectively. Each product occupies a row in Figures 2 and 3 representing the seasonal sum of the total bias E and its three components: hit bias H, missed precipitation $-M$, and false precipitation F, related by $E = H - M + F$.

[30] For the winter season (DFJ06), the six products share considerable similarities in their spatial distribution of the total bias and its three components. The most obvious common feature is the large areas of underestimates on either side of the continent and over the Rockies. These underestimates are attributed primarily to missed precipitation ($-M$) over these areas. The missed precipitation may be caused by snow cover on the ground at higher latitudes or over the Rockies, and by the inability to catch warm rain processes or short-lived convective storms at lower latitudes, or maritime precipitation along the west coast. Negative hit bias (H) also contributes to these underestimates, but it is largely confined along the west coast, and sometimes along the Appalachians (e.g., PERSIANN).

[31] On the other hand, many significant differences exist between these six products. AFWA and 3B42 exhibit smaller total bias (Figures 2a and 2b), especially over eastern CONUS. This shows the benefit of gauge data incorporation in these two algorithms. Also AFWA's missed precipitation is much less than other products, except the patches over the Rockies, whereas 3B42's particular gauge correction strategy cannot make up the rain undetected by the satellites. In addition, 3B42RT and NRL have remarkable overestimates over central CONUS, which are largely absent in other products. These overestimates can be traced to large false precipitation (Figure 2), with secondary contribution from hit bias. Both 3B42RT and NRL tend to have higher false precipitation for other three winter seasons (DJF04, 05, and 07, not shown here) as well, which is possibly caused by the particular calibration algorithms between IR and PMW used in both products. Finally, AFWA has some spotty false precipitation patterns near the northern border, and we determined they were caused by the sparse surface gauge data overlaid with the Barnes analysis scheme employed in AFWA.

[32] For the winter season missed precipitation is apparently the dominant error source for all these satellite-based products (except AFWA). We speculate this is mostly linked to the inability to measure snowfall, or rainfall over snow/ice-covered land surfaces with PMW, or it is often associated with low-level cloudiness and warm rain processes which may not have a strong signature of ice particles. The quantitative differences in the amount of missed precipitation should be related to the different screening strategies for land pixels. For example, CMORPH uses the daily snow cover to mask out anomalously high PMW rainfall, while TMPA products use PMW channels for the screening.

[33] For the summer season (JJA06, Figure 3), every product shows a very different picture from its winter counterpart. However, except for 3B42, the similarity of the error features between these products is still remarkable. Large-scale overestimates in total bias occupy central CONUS (eastern CONUS for AFWA), and heavy underestimates take place over New England and, to a less extent, the northwest. Both the overestimates and underestimates are mostly from hit biases (Figure 3). Both missed and false precipitation are much smaller, with the former concentrated largely along the Atlantic and Gulf coast, probably caused by undersampling of short-lived thunderstorms, and the latter scattered inland (e.g., 3B42RT, Figure 3c). AFWA does not seem to have benefited much from its gauge data correction for this season.

[34] TMPA 3B42 (Figure 3b) is qualitatively different from others. Its total biases are dominated by underestimates instead, with some scattered patches of slight overestimates in the midwest and the south of Ohio Valley. Still, most of these errors are from hit biases, with some en-

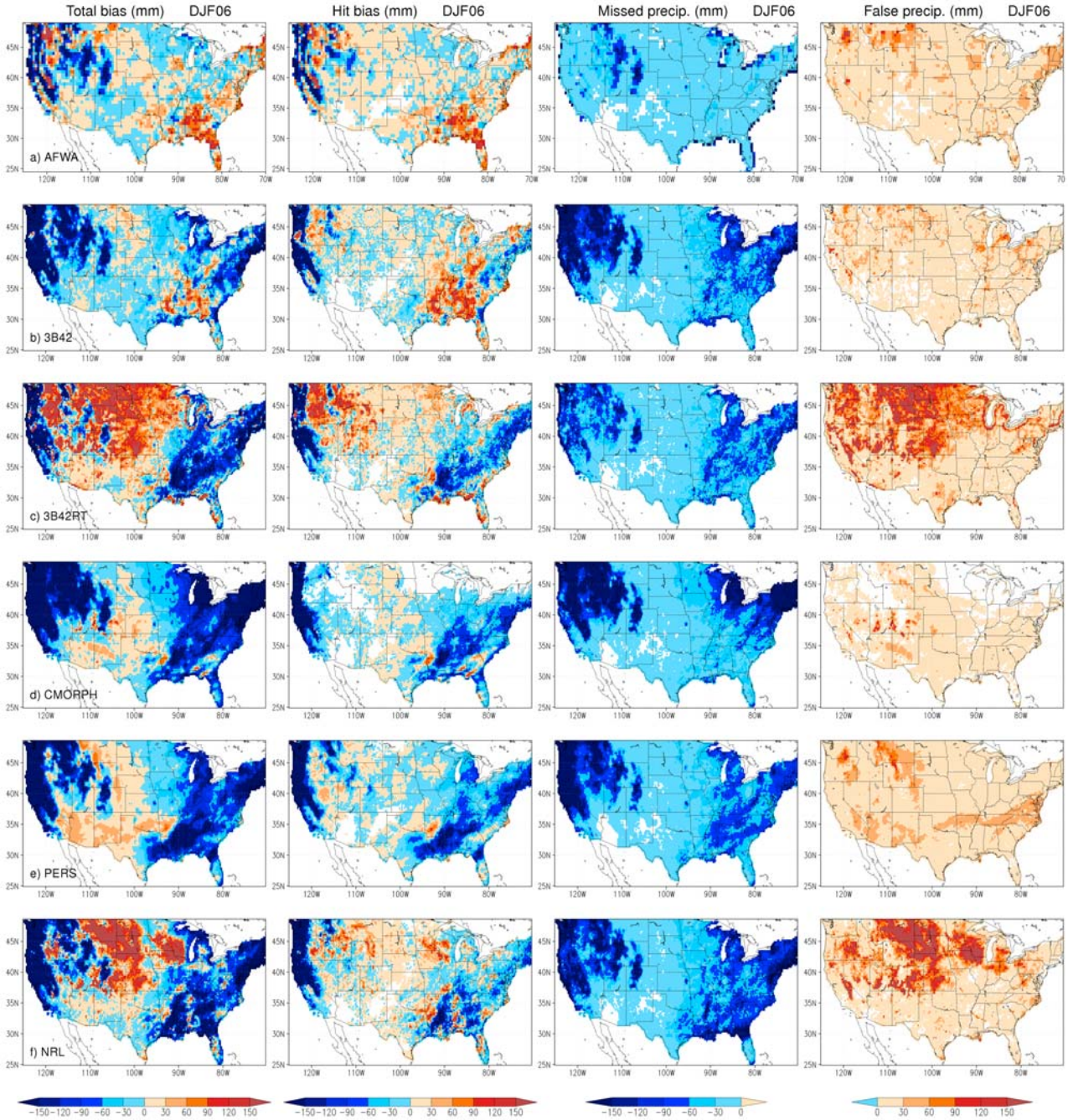

Figure 2. Error components of the six (6) data sets for the winter of 2006 (DJF06): total bias (E), hit bias (H), missed precipitation ($-M$), and false precipitation (F). The components are related by $E = H - M + F$.

hancement from missed precipitation for the underestimates, and from false precipitation for the overestimates, over different regions. The different hit bias feature from its real-time product, 3B42RT, illustrates the effect of its correction scheme with gauge data. False precipitation, overall, is not very pronounced for this season for 3B42, partly because the gauge correction scheme can effectively suppress this error component.

[35] In summary, the error decomposition enables one to better identify the error sources and their contributions to the total errors. The six data sets have rather different and unique error characteristics; meanwhile, some of their error components share considerable similarities despite their rather different algorithms. In the winter of DJF06, a remarkable amount of precipitation is consistently missed over either side of CONUS, except AFWA, and over the Rocky Mountains area in all the six data sets (Figures 2). In the summer of JJA06 (Figure 3), total biases in each data set tend to be dominated by strong overestimates from hit biases around central CONUS, except 3B42 (Figure 3b). The errors in hit biases in 3B42 were effectively alleviated by its gauge adjustment (Figure 3b). Substantial negative hit

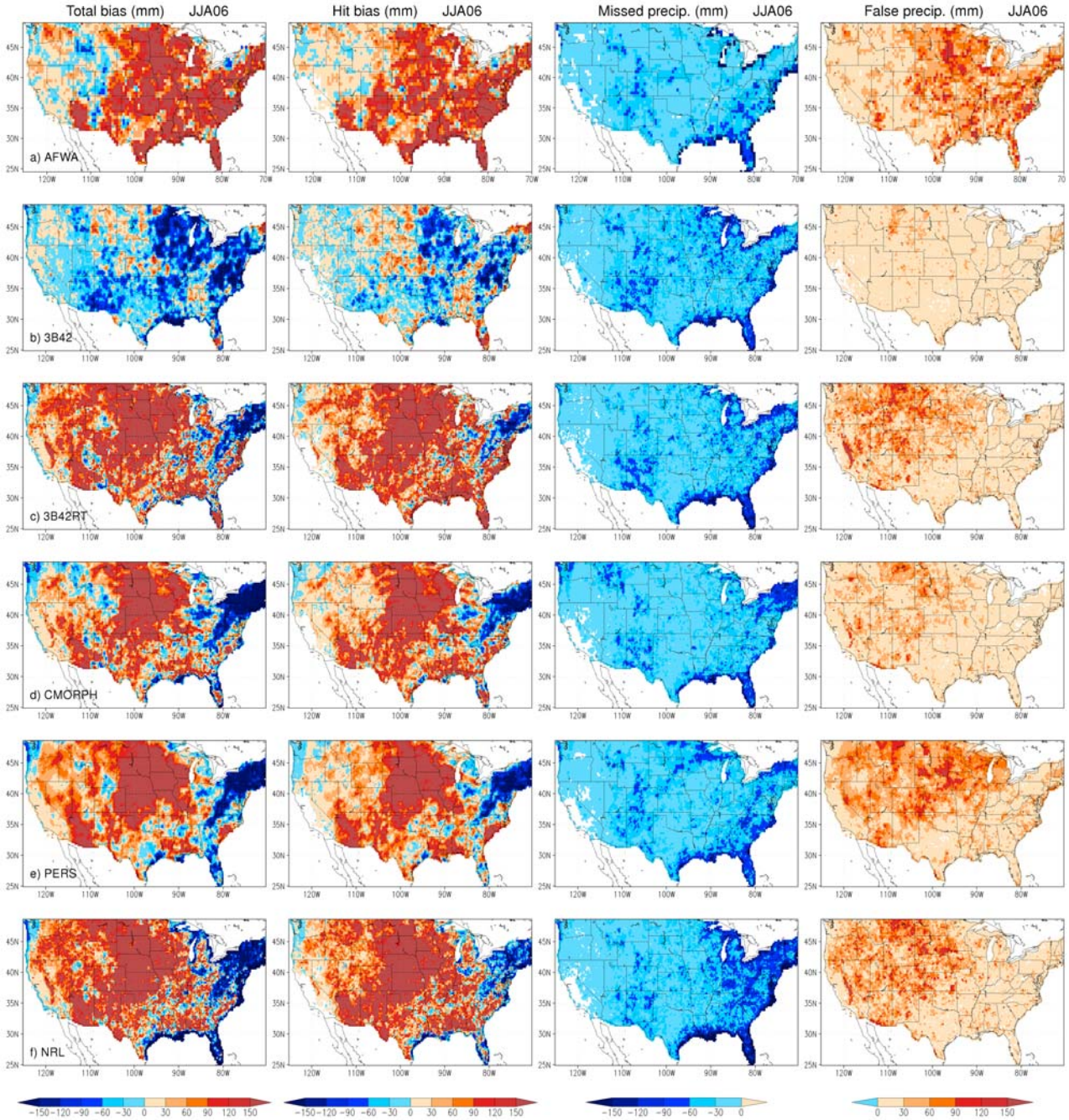

Figure 3. Same as Figure 2, except for the summer of 2006 (JJA06).

biases over New England and widespread missed precipitation over the eastern United States are also common features shared by all products except AFWA during summer (Figures 3b–3f). Overall, the last four products (3B42RT, CMORPH, PERSIANN and NRL, Figures 3c–3f) have much more similar spatial patterns in every error component than the other two products (AFWA and 3B42), and than their winter counterparts (Figure 2). These observations also apply roughly to other winters and summers (not shown here), except for the last winter of PERSIANN, which shows anomalously higher false precipitation which the data producers are currently investigating (also see section 4.2).

4.2. Temporal Analysis of Error Components

[36] To see the error characteristics of the six data sets over our entire study period, we also studied the daily error components as functions of time from July 2003 through February 2007. We divided CONUS into a western half and eastern half along the 100th meridian west, as previous studies show the two regions tend to have distinct error characteristics [*Gottschalck et al.*, 2005; *Ebert et al.*, 2007; *Tian et al.*, 2007]. Figure 4 shows the area-averaged error components as well as the total bias over the western (United States–west; Figure 4, left) and eastern (United States–east; Figure 4, right) half of CONUS, for the six data

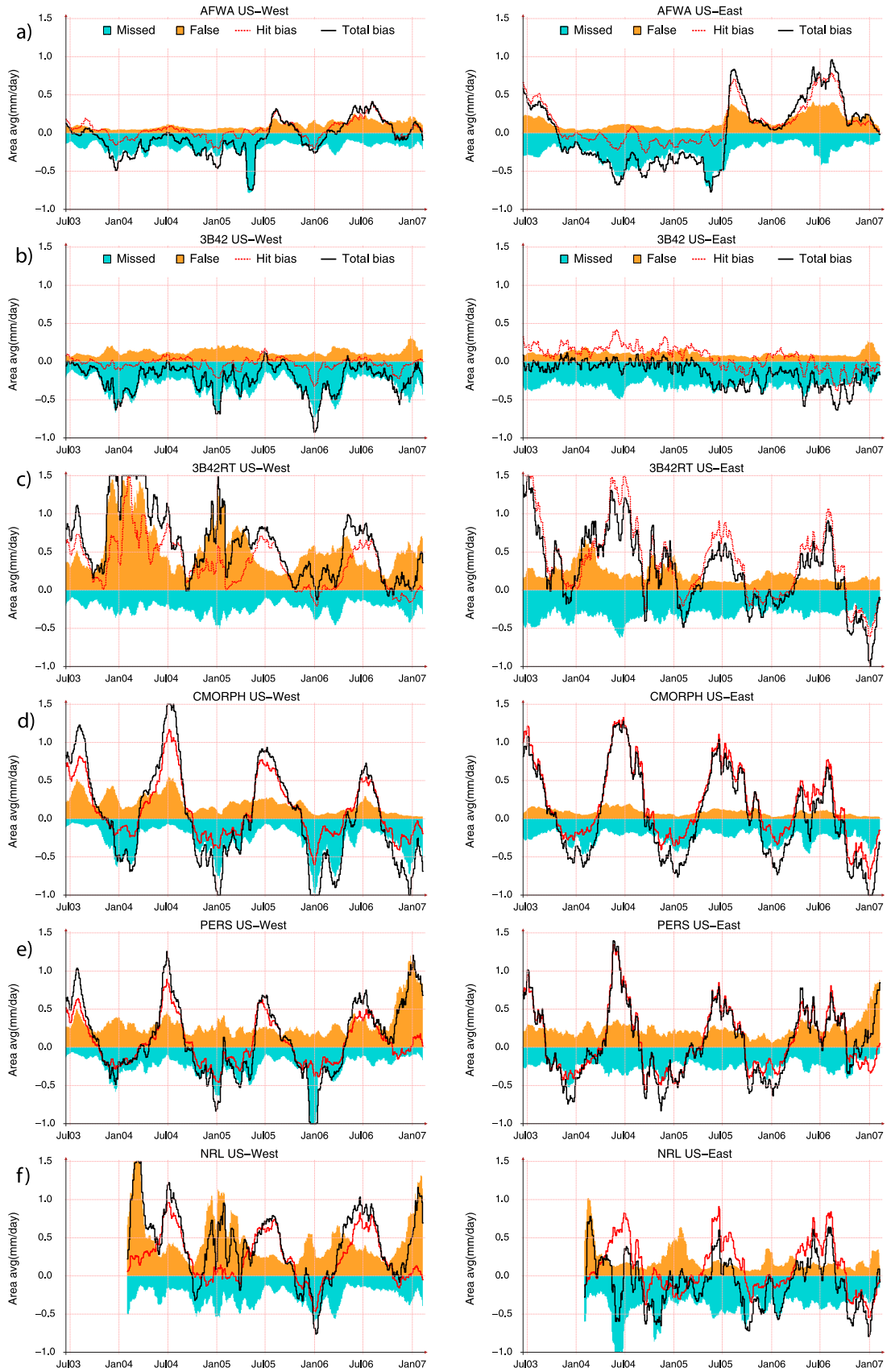

Figure 4. Time series of the error components, spatially averaged over the United States (left) west and (right) east. The two regions are separated by the 100th meridian west. A 31 day running average is applied to each time series to reduce visual cluttering.

sets. A 31 day running average is applied to each time series for smoothing and reducing visual cluttering.

[37] AFWA (Figures 4a) features considerable year-to-year variations without obvious systematic trend. In the west (Figure 4a, left), AFWA shows slight negative total bias (black line) during the first 2 years, with higher amplitudes in winter. Then it jumps to positive during the two last summers, but drops back to slight negative bias during the two intervening winters. During the first 2 years, the total bias is primarily from missed precipitation (turquoise area), as the other two components, false precipitation (orange area) and hit bias (red line), are considerably small. But during the last 1.5 years, false precipitation increases to a slightly higher amplitude than missed precipitation, and the two largely cancel each other. Subsequently, the total errors are dominated by hit bias, which is also responsible for the seasonal variation.

[38] In the east (Figure 4a, right), AFWA starts off in the first few months with hit bias-dominated errors. Both missed and false precipitation components are rather high but they counter each other. The following two summers (JJA04 and 05) see increased missed precipitation and decreased false precipitation and hit bias, and consequently, total errors are mostly caused by missed precipitation. During the last 1.5 years the reduced missed precipitation is canceled by strengthened false precipitation, and the total errors are close to hit bias. The large positive total bias during the last summer (JJA06) is consistent with the spatial patterns shown in Figure 3a.

[39] For 3B42 (Figure 4b), the most outstanding features are the nearly regular seasonal variation of missed precipitation in the west (Figure 4b, left, turquoise area), and the extremely small total bias in the east during the first 1.5 years (Figure 4b, right, black line). In the west, hit bias (red line) is rather small, and it counterbalances most of false precipitation (orange area). Consequently, total errors are largely controlled by missed precipitation, especially during the four winters. In the east, both missed and false precipitation are nearly constant, and in the first 1.5 years, missed precipitation is countered by the sum of hit bias and false precipitation, leading to very small total errors (black line). But the last 2 years start to see a drift to total underestimates, due to a shift of hit bias from positive to mostly negative. This is caused by a switch of gauge data source from the Global Precipitation Climatology Centre data set to CPC's Climate Anomaly Monitoring System data set.

[40] The four satellite-only data sets, 3B42RT, CMORPH, PERSIANN and NRL (Figures 4c–4f) have qualitatively different characteristics from either AFWA or 3B42 shown above, and share some major similarities among themselves. All of them have dramatic seasonal dependence in its error characteristics in both the west and east. Hit biases (red lines) dominate the total errors in summer. Most of them have strong positive hit bias in summer and low negative hit bias in winter. Another interesting common feature is the enhanced missed precipitation during winter in the west, with 3B34RT being the least pronounced. This behavior is also shared by 3B42 (Figure 4b). In the east, such seasonal variation of missed precipitation is not significant, and the amplitude is close to that of false precipitation (e.g., Figure 4b, left). Also note the reduced false precipitation in 3B42RT after the update of its algorithm starting in February 2005.

[41] Consequently, the net outcome of the three components' interplay is strong seasonal cycles of total errors, with overestimates in summer, mainly caused by positive hit biases, and underestimates in winter, caused by missed precipitation and negative hit biases, with the former dominating in the west. But there are exceptions. For example, 3B42RT (Figure 4c), has very strong false precipitation in the west during winter, and consequently overestimates are also large during winter, albeit from a different error component. Another example is PERSIANN (Figure 4e), which has anomalously high false precipitation dominating the total bias for the last winter (DJF07) in both the west and the east. Nevertheless, there are abundant examples to illustrate that sometimes the components work together to enhance the total errors (e.g., CMORPH Jul04, Figure 4d), while other times they cancel one another, resulting in much smaller total errors than most of their components (e.g., 3B42RT Jan06, Figure 4c).

[42] To summarize, Table 2 shows the seasonally averaged amplitudes of these error components and the total errors, as percentages of the total observed (Higgins) precipitation. For summer, hit bias (H) is generally the major contributor to the total errors, sometimes accounting for about 50% of the total precipitation (3B42RT and CMORPH). Missed precipitation ($-M$) and false precipitation (F) have similar amplitudes but are about two thirds smaller than hit bias. For winter, missed precipitation is the dominant source of errors, and is often much larger than total errors (e.g., 3B42 and NRL). False precipitation for 3B42RT and NRL is also particularly large, even higher than total errors too. In addition, these data sets will be rated differently by different criteria. For example, CMORPH has the highest amplitude in total biases in either winter or summer, but it has the lowest and second lowest false precipitation in winter and in summer, respectively.

4.3. Intensity Distribution of Error Components

[43] To look further into the nature of the error components, we computed the distribution of the components, as well as the total, as functions of daily precipitation intensity, as shown in Figure 5. The intensity distribution of the total precipitation for each of the six satellite-based products and for Higgins (R_2 and R_1 as in (3)) is shown in Figure 5a, and those of hit precipitation in the satellite-based products (H_2), missed precipitation ($-M$), and false precipitation (F) are shown in Figures 5b, 5c, and 5d, respectively. Each intensity distribution is computed over all the grid points over CONUS for the 4 winters (Figure 5, left) and 4 summers (Figure 5, right) (3 for NRL).

[44] For total precipitation (Figure 5a), the satellite-based data sets diverge from one another substantially. In winter (Figure 5a, left), NRL's distribution is closest to Higgins for intensities over 4 mm/d, and 3B42RT grossly overestimates for intensities over 10 mm/d. PERSIANN has more light precipitation (<10 mm/d) events and fewer strong (>10 mm/d) events than Higgins, while CMORPH constantly underestimates for all intensities. 3B42 first underestimates with intensities up to 30 mm/d, then gets close to Higgins for stronger precipitation. AFWA has a similar trend, but has tall spikes for intensities less than 20 mm/d

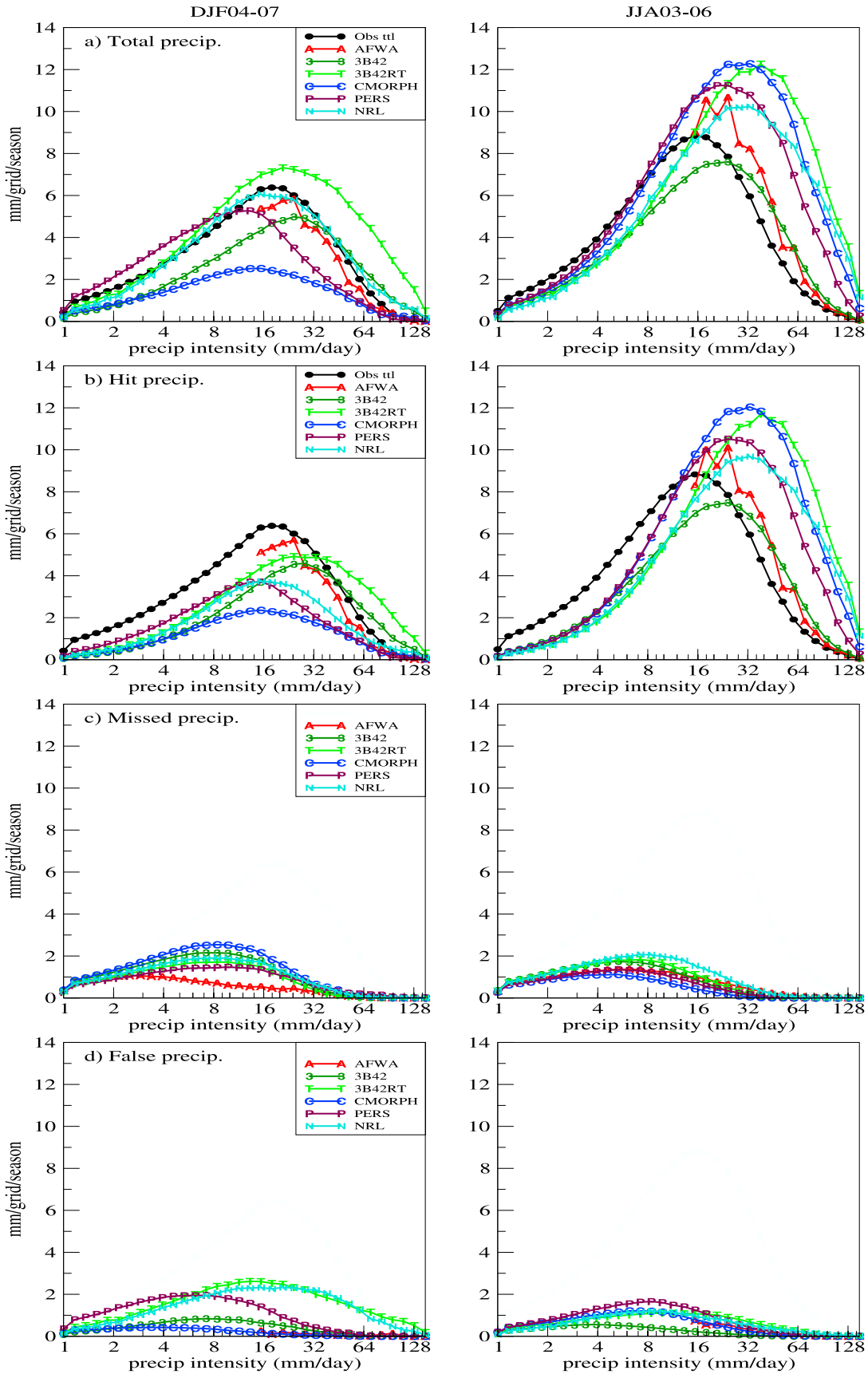

Figure 5. Intensity distribution of the error components for the six data sets. The results are computed from the (left) four winters and (right) four summers (three for NRL). The total observed (Higgins) precipitation (black line) is also shown in Figures 5a and 5b.

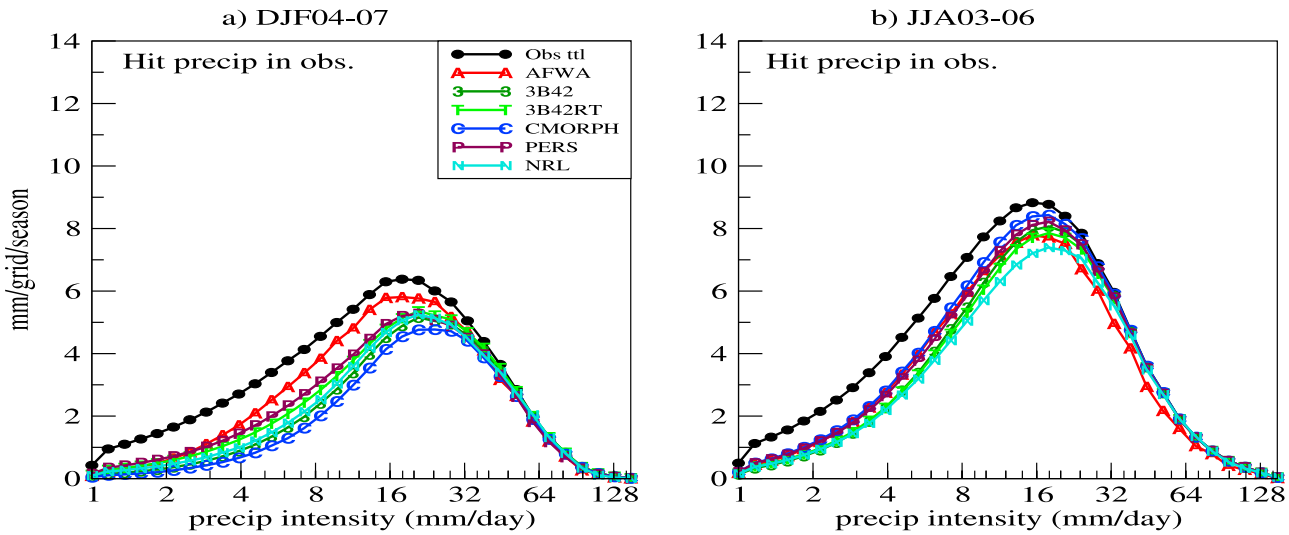

Figure 6. Intensity distribution of hit precipitation in observation (Higgins), H1.The results are computed from the (a) four winters and (b) four summers (three for NRL). The total observed (Higgins) precipitation (black line) is also shown.

(not shown to reduce cluttering). This seems to be caused by AFWA's rounding off of precipitation amounts to a few particular integers in millimeters.

[45] Figure 5b shows the intensity distribution of hit precipitation in satellite-based data, H_2, for winter (Figure 5b, left) and summer (Figure 5b, right). H_2 is essentially the total amount of precipitation from events coincidental with gauge-measured events. Overall they diverge remarkably from the observations and between one another as well. In winter, most products' hits underestimate except for 3B42RT and 3B42, which overestimate for strong events (>30 mm/d). In summer, all products dramatically overestimate strong events (>20 mm/d), especially for the 4 satellite-only products, 3B42RT, CMORPH, PERSIANN, and NRL. On the other hand, they consistently underestimate light events (<10 mm/d).

[46] Figures 5c and 5d show the other two error components: missed precipitation and false precipitation. The common feature between all the data sets and between the two seasons is that most missed and false precipitation is in the low-intensity range (1–10 mm/d). In addition, missed precipitation is slightly higher in winter than in summer (except for AFWA, Figure 5c). False precipitation for each product is also generally lower than its missed precipitation, but PERSIANN, 3B42RT, and NRL are exceptions in winter (Figure 5d). PERSIANN's false precipitation in summer is unusually slightly higher than others, presumably affected by the pattern shown in Figure 3e, while 3B42RT and NRL's have much broader distributions, extending to strong events (Figure 5d, left). In summer, false precipitation for each product is relatively low (Figure 5d, right).

[47] We also computed hit precipitation in Higgins (H_1 as in (4)), and show the results in Figure 6. Hit precipitation in observations (H_1), or in Higgins in particular here, enables one to see how much of the precipitation in Higgins are detected by each of the satellite-based estimates, and it essentially describes the detection rates by the satellite estimates for different observed intensities. Figure 6 shows H_1 (color lines) for both winter (Figure 6, left) and summer (Figure 6, right). The total precipitation in Higgins is also shown (black line) as reference. In either season, all the satellite-based products suffer from underestimates, especially for light precipitation (<20 mm/d) and for winter (Figure 6, left). For strong precipitation events (>20 mm/d), their detections are considerably improved, especially for summer (Figure 6, right). AFWA still slightly underestimates strong events for summer, but not for winter. For the detected precipitation events shown in Figure 6, the satellite-based products do not necessarily get the amplitudes (H_2) right, leading to hit bias ($H = H_2 - H_1$).

[48] In summary, all the six data sets captured strong rainfall events well. In both winter and summer, for precipitation intensity larger than 40mm/d, there are very few missed precipitation events, as manifested by both decreased missed precipitation (Figures 5c) and the little difference between hit precipitation and total precipitation in Higgins (Figure 6). Missed light precipitation, especially in winter, is a common problem. Within the intensity range of 2–10 mm/d, missed precipitation accounts for 50–80% of the observed total precipitation in winter (Figure 5c, left), and 20–50% in summer (Figure 5c, right).

5. Summary and Recommendations

[49] We studied the error characteristics of six leading satellite-based data sets, AFWA, 3B42, 3B42RT, CMORPH, PERSIANN, and NRL over CONUS for a period of 3.5 years (June 2003 to February 2007). We decomposed the total errors into three independent components: hit bias, missed precipitation and false precipitation, which have closer correspondence to the satellite-based retrieval processes. We are able to identify the contributions to the total errors from the three components, and their spatial and temporal features. This study yields new insights into the nature of the errors in these satellite-based estimates, including the following.

[50] 1. The total errors in each product result from the interplay of the three independent components. There are

many cases in which some of the error components are larger than the total errors. The components sometimes work together to enhance the total bias, but sometimes cancel one another to produce much smaller total bias (e.g., Figure 4c, January 2006).

[51] 2. The error sources, their geographical distribution, and their impacts are systematically different for different seasons. For example, during winter, missed precipitation is a major contributor to the total errors of 3B42RT, CMORPH, PERSIANN and NRL, up to 40%, especially over the Rocky Mountains (Figure 2). During summer, however, their total errors are dominated by hit biases spreading over most of CONUS (Figure 3), which overestimate as much as over 50%.

[52] 3. These satellite-based data sets perform reasonably well in detecting strong precipitation events (>40 mm/d), but it remains a challenge for them to get the amplitudes right; they all systematically overestimate the intensity in summer by a factor of 2 or more. In addition, they constantly miss about 20–80% of light precipitation (<10 mm/d). The amount of false precipitation also gets exceedingly large sometimes, especially for winter in the west (e.g., Figures 4c and 4f). The deficiencies in missed and false precipitation pose a common challenge to the majority of the products.

[53] 4. Incorporation of surface rain gauge data, such as in 3B42, helps to reduce total errors by adjusting the amplitudes of the hit biases and false precipitation. It also helps to bring the intensity distribution of heavy rainfall closer to the gauge data (Figure 5a), which will benefit surface runoff-related applications such as landslide forecast [*Hong et al.*, 2007]. Unfortunately this approach still does not affect missed precipitation because it, as well as other similar approaches such as probability matching [e.g., *Turk and Miller*, 2005] cannot generate undetected precipitation events in the system. In fact, 3B42 strives to minimize bias, and results in slightly boosted hit biases, to compensate for the missed precipitation. We also want to note the gauge data used in AFWA and 3B42 are essentially small and sparse subsets of the Higgins data set, so they are not totally independent but their information content is different. Our study shows a smaller number of gauges (AFWA) or long-term averages (3B42) can help to reduce a large portion of the bias, but also show the limitation of gauge correction, even if the gauge data used were perfect, because of missed precipitation in the original satellite data.

[54] 5. Missed precipitation in winter, especially over mountainous regions such as the Rockies, poses a common challenge for most of the products (e.g., Figure 2). The problem may be twice more severe than it appears here, because the ground reference data we used, Higgins, may be missing more than 50% of precipitation already [*Pan et al.*, 2003] because of the lower gauge density and because of the well-documented [e.g., *Legates and DeLiberty*, 1993] undercatch problem for rain gauges, especially during winter and in mountainous regions.

[55] We speculate the error characteristics of these products are primarily connected to the performance of PMW retrievals, because the six products, with rather different merging or blending algorithms, share remarkable similarity in error features, and *Ebert et al.* [2007] showed IR-PWM merged products are much more similar to PMW-only products than IR-only products. The summer positive hit biases in these products should be related to overestimates by PMW land algorithms for SSM/I, TMI and AMSR-E in convectively active regimes, while the winter negative hit biases should arise from underestimates in more stratiform precipitation [*McCollum and Ferraro*, 2003]. Additionally, PMW's inability to detect warm, topographically forced low-level rain and maritime precipitation without a strong ice signature may be responsible for the missed precipitation over the Rockies in summer and along the west coast in winter, respectively (Figures 2 and 3). Finally 3B42, 3B42RT, CMORPH, and NRL use AMSU-B in addition to other PMW sensors, which are expected to help with wintertime precipitation retrievals, but the current study does not show perceivable impacts. On the other hand, the techniques of merging IR and PMW do also contribute to the errors. For example, CMORPH's "morphing" algorithm improves the detection of rain events, leading to higher probability of detection, but with the price of overestimating rain amount in summer by smoothing out the intermittency in convective rain events, and possibly introducing more false precipitation. Conversely, the relatively low sampling frequency by PMW sensors could miss short-lived thunderstorms, and it could explain the high missed precipitation in the southeastern CONUS.

[56] We note that the failed detection of winter precipitation, presumably snowfall, is mostly due to the intrinsic inability to retrieve precipitation with PMW when the underlying land surface is covered by snow or ice [*Grody*, 1991; *Ferraro et al.*, 1998]. Therefore, these data sets simply report missing data or avoid using the PMW-based retrievals when such conditions exist.

[57] On the basis of our findings, we propose the following directions of improvement.

[58] 1. For all the six products, reduction of hit biases should be the easiest, particularly for heavy precipitation, and for summer. For the satellite-only products in particular (3B42RT, CMORPH, PERSIANN and NRL), it is imperative to reduce the gross overestimates over most part of CONUS during summer (Figure 5b, right).

[59] 2. Incorporation of snowfall retrieval data whenever they are available. Currently none of the products studied here includes snowfall retrievals. There have been research efforts for snowfall retrieval with different PMW frequency bands from the rainfall retrieval [e.g., *Kongoli et al.*, 2003; *Skofronick-Jackson et al.*, 2004]. Once such data are in production, all the products should strive to incorporate them. We believe this strategy will not only alleviate the deficiency of missed precipitation in winter, but also help get the intensity distribution right when gauge-based corrections are used (e.g., 3B42). Better snowfall detection in these products will also be critical to land surface hydrological studies involving snowpack accumulation and melting.

[60] 3. AFWA has spotty false precipitation features (e.g., Figure 2) resulting from its objective analysis of surface gauge reports. The nearly circular pattern of these spots is related to the isotropic weighting used in the *Barnes* [1964] scheme. Better blending of gauge data with satellite retrievals would help to reduce the impact. In addition, for PMW-based retrievals, AFWA currently only employs the SSM/I platforms. We recommend incorporation of retrievals from

newer PMW platforms, including SSMIS, TRMM, AMSR and AMSU, for improved coverage and accuracy.

[61] We want to note that though these error components can show better correspondence to the retrieval steps than more conventional approaches, the current analysis still can only provide evidence and feedback for data producers to infer the sources of error in their products; it is not possible to directly attribute or connect any part of the errors shown in this study to any specific sensors or processing stages. This is simply because most of the end products do not contain the information for tracking back the error to individual sensors, such as the weightings of the various sensors. Additionally, the merging, or blending of PMW, IR and surface gauges is by itself a complex and unique process for each product, and the errors introduced during this stage could be large enough to obscure the contribution from a specific sensor input. Recently, *Turk et al.* [2009] performed controlled experiments with NRL data set by adding or deleting certain input sensors and studied the impact on the end product. They found the overall quality of the end product is not particularly sensitive to one or the other type of PMW sensors added or deleted. Therefore we would propose an experiment for future studies: Have all of the algorithm developers used the identical exact input data sets for, say, three months during winter and three months during summer, and without any gauge adjustments. Then differences would presumably be due to the method of blending/transporting, since all of the physical adjustments (PMW data) would be the same. Then repeat the process with one or more PMW data sets added and/or improved. This approach should be able to isolate the effect of the PMW data and their algorithm characteristics from the details of each blending/merging technique.

[62] **Acknowledgments.** This research was supported in part by the NASA Precipitation Measurement Missions Program and the Terrestrial Hydrology Program under solicitation NRA-02-OES-05 (PI: Peters-Lidard) and the Air Force Weather Agency MIPR F2BBAJ6033GB01 (PI: Peters-Lidard). The authors wish to thank Mathew Sapiano, Dan Braithwaite, Ying Lin, Pingping Xie, and Yelena Yarosh for assistance with data access and questions and three anonymous reviewers for their in-depth comments and suggestions.

References

Adler, R. F., C. Kidd, G. Petty, M. Morissey, and H. M. Goodman (2001), Intercomparison of global precipitation products: The Third Precipitation Intercomparison Project (PIP-3), *Bull. Am. Meteorol. Soc.*, *82*, 1377–1396, doi:10.1175/1520-0477(2001)082<1377:IOGPPT>2.3.CO;2.

Arkin, P., and J. Turk (2006), Program to evaluate high resolution precipitation products (PEHRPP): A contribution to GPM planning, paper presented at 6th GPM International Planning Workshop, NASA, Annapolis, Md.

Arkin, P. A., and P. P. Xie (1994), The global precipitation climatology project: First Algorithm Intercomparison Project, *Bull. Am. Meteorol. Soc.*, *75*, 401–419, doi:10.1175/1520-0477(1994)075<0401:TGPCPF>2.0.CO;2.

Barnes, S. L. (1964), A technique for maximizing details in numerical weather map analysis, *J. Appl. Meteorol.*, *3*, 396–409, doi:10.1175/1520-0450(1964)003<0396:ATFMDI>2.0.CO;2.

Berg, W., T. L'Ecuyer, and C. Kummerow (2006), Rainfall climate regimes: The relationship of regional TRMM rainfall biases to the environment, *J. Appl. Meteorol. Climatol.*, *45*, 434–454, doi:10.1175/JAM2331.1.

Chen, M., W. Shi, P. Xie, V. B. S. Silva, V. E. Kousky, R. W. Higgins, and J. E. Janowiak (2008), Assessing objective techniques for gauge-based analyses of global daily precipitation, *J. Geophys. Res.*, *113*, D04110, doi:10.1029/2007JD009132.

Cressman, G. F. (1959), An operational objective analysis system, *Mon. Weather Rev.*, *87*, 367–374, doi:10.1175/1520-0493(1959)087<0367:AOOAS>2.0.CO;2.

Ebert, E. E., and J. L. McBride (2000), Verification of precipitation in weather systems: Determination of systematic errors, *J. Hydrol.*, *239*, 179–202, doi:10.1016/S0022-1694(00)00343-7.

Ebert, E. E., M. J. Manton, P. A. Arkin, R. J. Allam, G. E. Holpin, and A. J. Gruber (1996), Results from the GPCP Algorithm Intercomparison Programme, *Bull. Am. Meteorol. Soc.*, *77*, 2875–2887, doi:10.1175/1520-0477(1996)077<2875:RFTGAI>2.0.CO;2.

Ebert, E. E., J. E. Janowiak, and C. Kidd (2007), Comparison of near-real-time precipitation estimates from satellite observations and numerical models, *Bull. Am. Meteorol. Soc.*, *88*, 47–64, doi:10.1175/BAMS-88-1-47.

Ferraro, R. R., E. A. Smith, W. Berg, and G. J. Huffman (1998), A screening methodology for passive microwave precipitation retrieval algorithms, *J. Atmos. Sci.*, *55*, 1583–1600, doi:10.1175/1520-0469(1998)055<1583:ASMFPM>2.0.CO;2.

Gottschalck, J., J. Meng, M. Rodell, and P. Houser (2005), Analysis of multiple precipitation products and preliminary assessment of their impact on Global Land Data Assimilation System land surface states, *J. Hydrometeorol.*, *6*, 573–598, doi:10.1175/JHM437.1.

Grody, N. C. (1991), Classification of snow cover and precipitation using the Special Sensor Microwave Imager, *J. Geophys. Res.*, *96*, 7423–7435, doi:10.1029/91JD00045.

Higgins, R. W., W. Shi, and E. Yarosh (2000), Improved United States precipitation quality control system and analysis, 40 pp., Natl. Cent. for Environ. Predict., Camp Springs, Md.

Hong, Y., R. F. Adler, F. Hossain, S. Curtis, and G. J. Huffman (2007), A first approach to global runoff simulation using satellite rainfall estimation, *Water Resour. Res.*, *43*, W08502, doi:10.1029/2006WR005739.

Hossain, F., and G. J. Huffman (2008), Investigating error metrics for satellite rainfall data at hydrologically relevant scales, *J. Hydrometeorol.*, *9*, 563–575, doi:10.1175/2007JHM925.1.

Hsu, K., X. Gao, S. Sorooshian, and H. V. Gupta (1997), Precipitation estimation from remotely sensed information using artificial neural networks, *J. Appl. Meteorol.*, *36*, 1176–1190, doi:10.1175/1520-0450(1997)036<1176:PEFRSI>2.0.CO;2.

Hsu, K., H. V. Gupta, X. Gao, and S. Sorooshian (1999), Estimation of physical variables from multi-channel remotely sensed imagery using a neural network: Application to rainfall estimation, *Water Resour. Res.*, *35*, 1605–1618, doi:10.1029/1999WR900032.

Huffman, G. J., R. F. Adler, P. Arkin, A. Chang, R. Ferraro, A. Gruber, J. Janowiak, A. McNab, B. Rudolph, and U. Schneider (1997), The Global Precipitation Climatology Project (GPCP) combined precipitation dataset, *Bull. Am. Meteorol. Soc.*, *78*, 5–20, doi:10.1175/1520-0477(1997)078<0005:TGPCPG>2.0.CO;2.

Huffman, G. J., R. F. Adler, D. T. Bolvin, G. Gu, E. J. Nelkin, K. P. Bowman, Y. Hong, E. F. Stocker, and D. B. Wolff (2007), The TRMM Multi-satellite Precipitation Analysis (TMPA): Quasi-global, multi-year, combined-sensor precipitation estimates at fine scales, *J. Hydrometeorol.*, *8*, 38–55, doi:10.1175/JHM560.1.

Huffman, G. J., R. F. Adler, D. T. Bolvin, and E. J. Nelkin (2009), The TRMM Multi-satellite Precipitation Analysis (TMPA), in *Satellite Applications for Surface Hydrology*, edited by F. Hossain and M. Gebremichael, Springer, New York, in press.

Janowiak, J. E., V. E. Kousky, and R. J. Joyce (2005), Diurnal cycle of precipitation determined from the CMORPH high spatial and temporal resolution global precipitation analyses, *J. Geophys. Res.*, *110*, D23105, doi:10.1029/2005JD006156.

Joyce, R. J., J. E. Janowiak, P. A. Arkin, and P. Xie (2004), CMORPH: A method that produces global precipitation estimates from passive microwave and infrared data at high spatial and temporal resolution, *J. Hydrometeorol.*, *5*, 487–503, doi:10.1175/1525-7541(2004)005<0487:CAMTPG>2.0.CO;2.

Kidd, C., D. R. Kniveton, M. C. Todd, and T. J. Bellerby (2003), Satellite rainfall estimation using combined passive microwave and infrared algorithms, *J. Hydrometeorol.*, *4*, 1088–1104, doi:10.1175/1525-7541(2003)004<1088:SREUCP>2.0.CO;2.

Kongoli, C., P. Pellegrino, R. Ferraro, N. Grody, and H. Meng (2003), A new snowfall detection algorithm over land using measurements from the Advanced Microwave Sounding Unit (AMSU), *Geophys. Res. Lett.*, *30*(14), 1756, doi:10.1029/2003GL017177.

Legates, D., and T. DeLiberty (1993), Precipitation measurement biases in the United States, *Water Resour. Bull.*, *29*, 855–861.

Lin, Y., and K. E. Mitchell (2005), The NCEP stage II/IV hourly precipitation analyses: Development and applications, paper presented at 19th Conference on Hydrology, Am. Meteorol. Soc., San Diego, Calif.

McCollum, J. R., and R. R. Ferraro (2003), Next generation of NOAA/NESDIS TMI, SSM/I, and AMSR-E microwave land rainfall algorithms, *J. Geophys. Res.*, *108*(D8), 8382, doi:10.1029/2001JD001512.

Nijssen, B., and D. Lettenmaier (2004), Effect of precipitation sampling error on simulated hydrological fluxes and states: Anticipating the Global

Precipitation Measurement satellites, *J. Geophys. Res.*, *109*, D02103, doi:10.1029/2003JD003497.

Nykanen, D. K., E. Foufoula-Georgiou, and W. M. Lapenta (2001), Impact of small-scale rainfall variability on larger-scale spatial organization of land-atmosphere fluxes, *J. Hydrometeorol.*, *2*, 105–121, doi:10.1175/1525-7541(2001)002<0105:IOSSRV>2.0.CO;2.

Ogden, F. L., and P. Y. Julien (1993), Runoff sensitivity to temporal and spatial rainfall variability at runoff plane and small basin scale, *Water Resour. Res.*, *29*, 2589–2597, doi:10.1029/93WR00924.

Pan, M., et al. (2003), Snow process modeling in the North American Land Data Assimilation System (NLDAS): 2. Evaluation of model simulated snow water equivalent, *J. Geophys. Res.*, *108*(D22), 8850, doi:10.1029/2003JD003994.

Ruane, A. C., and J. O. Roads (2007), 6-hour to 1-year variance of five global precipitation sets, *Earth Interact.*, *11*, 1–29, doi:10.1175/EI225.1.

Sapiano, M. R. P., and P. A. Arkin (2009), An intercomparison and validation of high-resolution satellite precipitation estimates with 3-hourly gauge data, *J. Hydrometeorol.*, *10*, 149–166, doi:10.1175/2008JHM1052.1.

Skofronick-Jackson, G. M., M.-J. Kim, J. A. Weinman, and D.-E. Chang (2004), A physical model to determine snowfall over land by microwave radiometry, *IEEE Trans. Geosci. Remote Sens.*, *42*, 1047–1058, doi:10.1109/TGRS.2004.825585.

Smith, E. A., J. E. Lamm, R. F. Adler, J. Alishouse, and K. Aonashi (1998), Results of the WetNet PIP-2 project, *J. Atmos. Sci.*, *55*, 1483–1536, doi:10.1175/1520-0469(1998)055<1483:ROWPP>2.0.CO;2.

Sorooshian, S., K.-L. Hsu, X. Gao, H. V. Gupta, B. Imam, and D. Braithwaite (2000), Evaluation of PERSIANN system satellite-based estimates of tropical rainfall, *Bull. Am. Meteorol. Soc.*, *81*, 2035–2046, doi:10.1175/1520-0477(2000)081<2035:EOPSSE>2.3.CO;2.

Tian, Y., and C. D. Peters-Lidard (2007), Systematic anomalies over inland water bodies in satellite-based precipitation estimates, *Geophys. Res. Lett.*, *34*, L14403, doi:10.1029/2007GL030787.

Tian, Y., C. D. Peters-Lidard, M. Garcia, and S. Kumar (2006), Evaluation of TRMM-based precipitation products in the southeast U. S. and their impact on hydrological modeling, *Eos Trans. AGU*, *87*(36), Jt. Assem. Suppl., Abstract H23A–03.

Tian, Y., C. D. Peters-Lidard, B. J. Choudhury, and M. Garcia (2007), Multitemporal analysis of TRMM-based satellite precipitation products for land data assimilation applications, *J. Hydrometeorol.*, *8*, 1165–1183, doi:10.1175/2007JHM859.1.

Turk, F. J., and S. D. Miller (2005), Toward improving estimates of remotely sensed precipitation with MODIS/AMSR-E blended data techniques, *IEEE Trans. Geosci. Remote Sens.*, *43*, 1059–1069, doi:10.1109/TGRS.2004.841627.

Turk, F. J., G. V. Mostovoy, and V. Anantharaj (2009), Soil moisture sensitivity to NRL-blend high resolution precipitation products: Analysis of simulations with two land surface models, *IEEE J. Selec. Topics Appl. Earth Obs. Remote Sens.*, in press.

Vicente, G. A., R. A. Scofield, and W. P. Menzel (1998), The operational GOES infrared rainfall estimation technique, *Bull. Am. Meteorol. Soc.*, *79*, 1883–1898, doi:10.1175/1520-0477(1998)079<1883:TOGIRE>2.0.CO;2.

Wilks, D. S. (1995), *Statistical Methods in the Atmospheric Sciences*, 467 pp., Academic, San Diego, Calif.

R. F. Adler and G. J. Huffman, Laboratory for Atmospheres, NASA Goddard Space Flight Center, Code 613.1, Greenbelt, MD 20771, USA.

J. B. Eylander, Air and Space Models Integration Branch, Air Force Weather Agency, 101 Nelson Dr., Offutt Air Force Base, NE 68113-1023, USA.

M. Garcia, Department of Hydrology and Water Resources, University of Arizona, Tucson, AZ 85721, USA.

K. Hsu, Center for Hydrometeorology and Remote Sensing, Department of Civil and Environmental Engineering, University of California, Irvine, CA 92697-2175, USA.

R. J. Joyce, Climate Prediction Center, NCEP, NWS, NOAA, Camp Springs, MD 20746, USA.

C. D. Peters-Lidard, Y. Tian, and J. Zeng, NASA Goddard Space Flight Center, Mail Code 614.3, Greenbelt, MD 20771, USA. (yudong.tian@nasa.gov)

F. J. Turk, Marine Meteorology Division, Naval Research Laboratory, Monterey, CA 93943-5502, USA.